THE ASTROPHYSICAL JOURNAL, 485:112–124, 1997 August 10

UNIFICATION OF THE RADIO AND OPTICAL PROPERTIES OF GIGAHERTZ PEAK SPECTRUM AND COMPACT STEEP-SPECTRUM RADIO SOURCES

GEOFFREY V. BICKNELL,[1] MICHAEL A. DOPITA,[2] AND CHRISTOPHER P. O. O'DEA[3]
Received 1996 October 2; accepted 1997 February 7

ABSTRACT

We adopt the view that the classes of active galactic nuclei (AGN) known variously as gigahertz peak spectrum (GPS) sources, compact steep-spectrum (CSS) sources, and compact symmetric objects (CSO) generally represent the same sort of object and show that both their radio spectra and optical emission can be explained by a single model which incorporates the effects produced by the interaction of a jet-driven nonthermal lobe with a dense interstellar medium. Following Begelman, we assume that these sources are young AGNs (ages $\lesssim 10^6$ yr) in which the jets are propagating through an interstellar medium in which the hydrogen number density, $n_{\rm H}$ decreases as a power law with radius, with the index $\delta \approx 1$–2 and $n_{\rm H} \sim 10$–100 cm^{-3} at 1 kpc. The bow shock preceding the radio lobe is radiative at early times in such a dense environment, and the optical line emission produced by the shocked ISM and the associated photoionized precursor is proportional to the monochromatic radio power, consistent with the observational data of Gelderman & Whittle. The ionized gas surrounding the lobes has a significant emission measure and a correspondingly high free-free opacity which is responsible for the 0.1–1 GHz peaks in the radio spectra. For jet energy fluxes $\sim 10^{45}$–10^{46} ergs s^{-1}, consistent with the observed radio powers of these objects, the crucial observed anticorrelation between peak frequency and size is readily recovered. The form of the radio spectra (power laws at high and low frequencies) indicate that the absorption is due to a cloudy/filamentary medium with an approximately uniform distribution of opacities resulting from a combination of a two-phase interstellar medium, shock shredding of clouds impacted by the bow shock and thermal instabilities in the shocked ISM. The ionized medium enveloping the radio source also forms a Faraday screen which produces high rotation measure and substantial depolarization, readily accounting for another key property of this class of AGNs.

Subject headings: radio continuum: galaxies

1. INTRODUCTION

There has been an increasing amount of interest over the last few years in the classes of extragalactic radio sources known as compact symmetric objects (CSOs: Wilkinson et al. 1994; Readhead et al. 1996), gigahertz peaked spectrum (GPS) sources (e.g., O'Dea, Baum, & Stranghellini 1991), and compact steep-spectrum sources (CSS; e.g., Fanti et al. 1990), although the research on these objects can be traced back to the work on "Compact Doubles" (Phillips & Mutel 1982) which are a subset of the above classes (Fanti et al. 1990). Following the Caltech-Jodrell Bank (Wilkinson et al. 1994) and Bologna-Jodrell-Dwingeloo surveys (Fanti et al. 1995), these classes of radio sources are now understood to represent an appreciable fraction of luminous radio sources. For example, GPS sources constitute approximately 24% of the Molonglo quasar catalog (Baker, Hunstead, & Brinkmann 1995). For the most part, the separate classes probably represent the same sort of object, the different nomenclature being more indicative of the means of discovery rather than of a real physical difference. CSOs have emerged as a distinct morphological class in VLBI surveys; their morphology and power is typical of classic double-lobed radio sources, albeit on subgalactic ($\sim$100 pc to 1 kpc scale). Moreover, without any exception known to us, every CSO is a GPS source. The converse is not exactly true: there are examples of GPS sources with somewhat distorted morphologies (Dallasca et al. 1995; Stranghellini et al. 1996a), and these are therefore inconsistent with the "symmetric" part of the CSO definition. Nevertheless, in the context of the model presented in this paper this is probably the result of interaction with an ISM which is more inhomogeneous than that in the average CSO or GPS source. For the most part, therefore, GPS sources and CSOs are quite different from the more numerous, relativistically beamed, core-jet sources. CSS sources have steep spectra ($\alpha \gtrsim 0.5$)[4] at gigahertz frequencies (in contrast to many quasars the spectra of which are flat in this frequency range). However, studies of the radio spectra of CSS sources (Fanti et al. 1990, 1985, 1989; Kameno et al. 1995) have demonstrated the existence of a turnover at lower frequencies ($\sim$100 MHz) for many CSS sources demonstrating, in all likelihood, that GPS and CSS sources differ in degree rather than kind.

Scenarios for these sources generally suppose that they are either young, or frustrated in their growth by dense ambient nuclear material (or both) and that the spectral peak results from synchrotron self-absorption (SSA) by the lobe plasma. The SSA model to explain the low-frequency slope of radio sources has been a popular one, especially in view of its success in explaining the spectra of core-jet sources (Blandford & Königl 1979). Nevertheless, early in the history of the subject of GPS and CSS sources, van Breugel (1981) pointed out that the emission measure of ionized gas implied by the flux of narrow line emission from

[1] Astrophysical Theory Centre, Australian National University, Canberra, ACT 0200, Australia. The ANUATC is operated jointly by the Mount Stromlo and Siding Spring Observatories and the School of Mathematical Sciences; gvb@maths.anu.edu.au.

[2] Mount Stromlo and Siding Spring Observatories, Weston PO, ACT 2611, Australia; mad@mso.anu.edu.au.

[3] Space Telescope Science Institute, 3700 San Martin Drive, Baltimore, MD; odea@stsci.edu.

[4] The spectral index α is defined by $F_\nu \propto \nu^{-\alpha}$.

CSS sources, implied that free-free absorption is an attractive explanation for the peak in the radio spectrum. Another simple argument against the SSA hypothesis is that if the properties of the jets in these sources are not substantially different from jets in core-dominated sources, then it would be suprising to find nonthermal plasma making the transition from optically thick to optically thin and then becoming optically thick again in the much more extensive lobes. Whatever the cause for the morphology and spectrum, the substantial representation of CSOs, GPSs, and CSSs in radio source catalogs implies that they represent an important phase in the evolution of all active galaxies.

A comprehensive physical model for these objects must explain the following properties:

1. Compact (0.1–10 kpc) symmetric radio lobes between which a core may or may not be seen and which, in the case of radio galaxies, show little if any sign of relativistic beaming. These lobes have the classical FR2 morphology, but at much smaller scales (Fanti et al. 1990; Wilkinson et al. 1994; Spencer et al. 1989; Sanghera et al. 1995; Dallacasa et al. 1995). Some indication of relativistic beaming, in the form of prominent jets, is found in CSS quasars (Fanti et al. 1990; Spencer et al. 1989; Sanghera et al. 1995).

2. Steeply rising ($\langle\alpha\rangle \approx -1$) low-frequency spectra, with flux density maxima in the region of 0.1–10 GHz, and with nonthermal high-frequency slopes $0.5 \lesssim \alpha \lesssim 1.3$ (e.g., Fanti et al. 1985, 1989; Kameno et al. 1995; O'Dea et al. 1990; Stanghellini et al. 1996b). The low-frequency spectral indices are *not* indicative of either a single-component synchrotron self-absorbed spectrum or a single-component free-free absorbed spectrum.

3. Very powerful radio emission [logarithmic mean power at 5 GHz, $\log (P_5/\mathrm{W\ Hz^{-1}}) \sim 27.5$] (Fanti et al. 1990; Stanghellini et al. 1996b).

4. An inverse relationship between source size and turnover frequency (Fanti et al. 1990; Stanghellini et al. 1996b; O'Dea & Baum 1996). As indicated above, this is a crucial relationship which serves to identify GPS, CSO, and CSS sources as one and the same class of object.

5. Low source polarization (typically $\lesssim 1\%$ in GPS sources and $\lesssim 3\%$ in CSS sources) accompanied in some cases by very high rotation measures (up to several thousand rad $\mathrm{m^{-2}}$) (O'Dea et al. 1990; Taylor, Inoue, & Tabara 1992; Stanghellini et al. 1996b; Akujor & Garrington 1995; Mantovani et al. 1994; Sanghera et al. 1995; Inoue et al. 1995).

6. Disturbed isophotes in the parent galaxies, pointing to recent interaction (Stanghellini et al. 1993; Gelderman 1994), with spectroscopy suggesting large quantities of dust indicating a dense galactic medium (Baker & Hunstead 1996).

7. Very luminous "narrow line" emission (up to $\sim 10^{44}$ ergs $\mathrm{s^{-1}}$). The [O III] luminosity of CSS sources is higher than that of other types of radio galaxies and the velocity widths are also systematically higher (up to ~ 2000 km $\mathrm{s^{-1}}$) (Gelderman & Whittle 1994, 1996).

8. There is a tight correlation between line luminosity and total radio power (Gelderman & Whittle 1996).

Begelman (1966) has recently presented an evolutionary model for CSO sources showing that the luminosity-size statistics can be explained if they are relatively young ($t \sim 10^6$ yr) and are forcing their way through a dense galactic medium in which the density decreases roughly as $r^{-\delta}$ with $\delta \approx 1.5$–2. In this model, CSOs are both young and, although frustrated in their growth by the ambient ISM, are not confined by it. In this paper, we build upon this model to show that the properties of GPS and CSS sources follow as a natural consequence of the radio lobe–ISM interaction. In our model, the strong radiative shocks which precede the advantage of the lobe into the ISM create an ionized shell of shocked ISM capable of free-free absorbing low-frequency radio emission, thereby causing the peak in the radio spectrum. The observed optical velocity dispersion in the model is determined by a combination of factors: the velocity dispersion in the "undisturbed" ISM, which emits the precursor emission; the geometry of the bubble, which determines the projection factors; and velocities in the photoabsorption-recombination region of the shock, which are effectively equal to the velocity of the shock preceding the bubble. As a consequence, the observed velocity width is not simply related to the shock velocity but is at least indicative of it. We therefore conclude, from the data of Gelderman & Whittle (1994), that we are dealing with radiative shocks in the approximate range 300–1000 km $\mathrm{s^{-1}}$.

2. DYNAMICS OF A JET-FED LOBE

2.1. *The Dynamical Model for the Lobe*

Clearly, the most important parameter for shock models, determining the shock luminosity and the emission-line ratios, is the velocity of the shock and this, in principle, is determined by the model for the jet-fed lobe. However, the standard model for a single fixed-direction jet feeding a lobe is insufficient: we know from the observational and theoretical studies of jets on the kiloparsec scale, that jets jitter about in the "dentist's drill" fashion envisaged by Scheuer (1982). This insight led to a number of papers involving numerical simulations of this process (e.g., Williams & Gull 1984; Gull, Cox, & Scheuer 1991; Clarke 1996; Norman 1996). Moreover, it is quite clear that the lobes in the most powerful radio sources are overpressured with respect to the ambient medium as a consequence of the thermalization of jet plasma by the terminating shock (see Begelman & Cioffi 1989). This feature and the dentist's drill evolution have been incorporated into an analytical model by Begelman (1996). In this model, allowance is made, in a phenomenological fashion, for the jittering of the jet as it feeds nonthermal plasma to the expanding lobe. The main assumption of the model is that the mean pressure, averaged over the hotspot region of the lobe is ζ times the average lobe pressure where $\zeta \approx 2$. De Young (1993) has also carried out numerical simulations of powerful jets propagating in dense environments aimed specifically at understanding the physics of CSS and GPS sources. Those simulations were axisymmetric and did not specifically involve a dentist drill effect. Nevertheless, De Young's conclusion that an evolving radio source interacts with a clumpy two-phase medium in a similar fashion to the way in which it would interact with a smooth medium with the same average density is relevant to our utilization of the Begelman model. The reason for this result is that impact of the radio source on individual clouds shreds them and creates a more uniform medium. Nevertheless, De Young assumed that the clouds are small compared to the jet radius, and it would be useful to carry out simulations involving clouds of larger relative sizes.

We have modified Begelman's treatment slightly to allow for the adiabatic expansion of the lobe plasma since this allows for a more internally consistent evaluation of the energy imparted to the ISM by the expanding lobe. In the evolution equations given below, the following symbols are used (see also Fig. 1): x_h, distance of hot spot from the center of the galaxy; r_c, maximum radius of the cocoon; pressure; V_c, cocoon volume; $E_c = 3P_c V_c$, total cocoon energy; β_j, (jet velocity)/c; F_E, jet energy flux; ρ_a, ambient density; A_h, averaged hot spot area. In terms of these parameters, the lobe evolution equations are

$$\frac{dx_h}{dt} \approx \left(\frac{\beta_j F_E}{\rho_a c A_h}\right)^{1/2} \approx \zeta^{1/2}\left(\frac{P_c}{\rho_a}\right)^{1/2} , \tag{2.1}$$

$$\frac{dr_c}{dt} \approx \left(\frac{P_c}{\rho_a}\right)^{1/2} , \tag{2.2}$$

$$\frac{dE_c}{dt} + P_c \frac{dV_c}{dt} \approx F_E . \tag{2.3}$$

These equations assume that the jet velocity is relativistic and that the cocoon pressure is dominated by relativistic particles. We further assume that the cocoon is semi-ellipsoidal with semimajor and semiminor axes x_h and r_c, respectively; hence, $V_c = 2\pi/3 x_h r_c^2$. The galactic ISM density is assumed to be a power law, with index $-\delta$ as a function of distance from the center. Neglecting the modest variation of background density over the (nonspherical) surface of the lobe, we take (following Begelman 1996) $\rho_a = \rho_0 (x_h/x_0)^{-\delta}$, where $x_0 = 1$ kpc is a fiducial distance and ρ_0 is the ISM density at 1 kpc. The one difference between the above equations and those of Begelman (1996) is that allowance has been made for adiabatic losses in the cocoon energy equation. This enables a more internally consistent approach to the calculation of the energy imparted to the interstellar medium by $P\,dV$ work in § 4.

2.2. *The Solution for Lobe Size and Pressure*

The above equations admit the following solutions for x_h and p_c as functions of time:

$$x_h = x_0\, \xi^{1/(5-\delta)} , \tag{2.4}$$

$$P_c = P_0\, \xi^{(2-\delta)/(5-\delta)} , \tag{2.5}$$

where

$$\xi = \frac{(5-\delta)^3 \zeta^2}{18\pi(8-\delta)} \left(\frac{F_E t^3}{\rho_0 x_0^5}\right) , \tag{2.6}$$

$$P_0(t) = \frac{9}{\zeta(5-\delta)^2}\, \rho_0 \left(\frac{x_0}{t}\right)^2 . \tag{2.7}$$

Expressing the solution in this way immediately provides a way of estimating the relevant jet energy flux, F_E and the

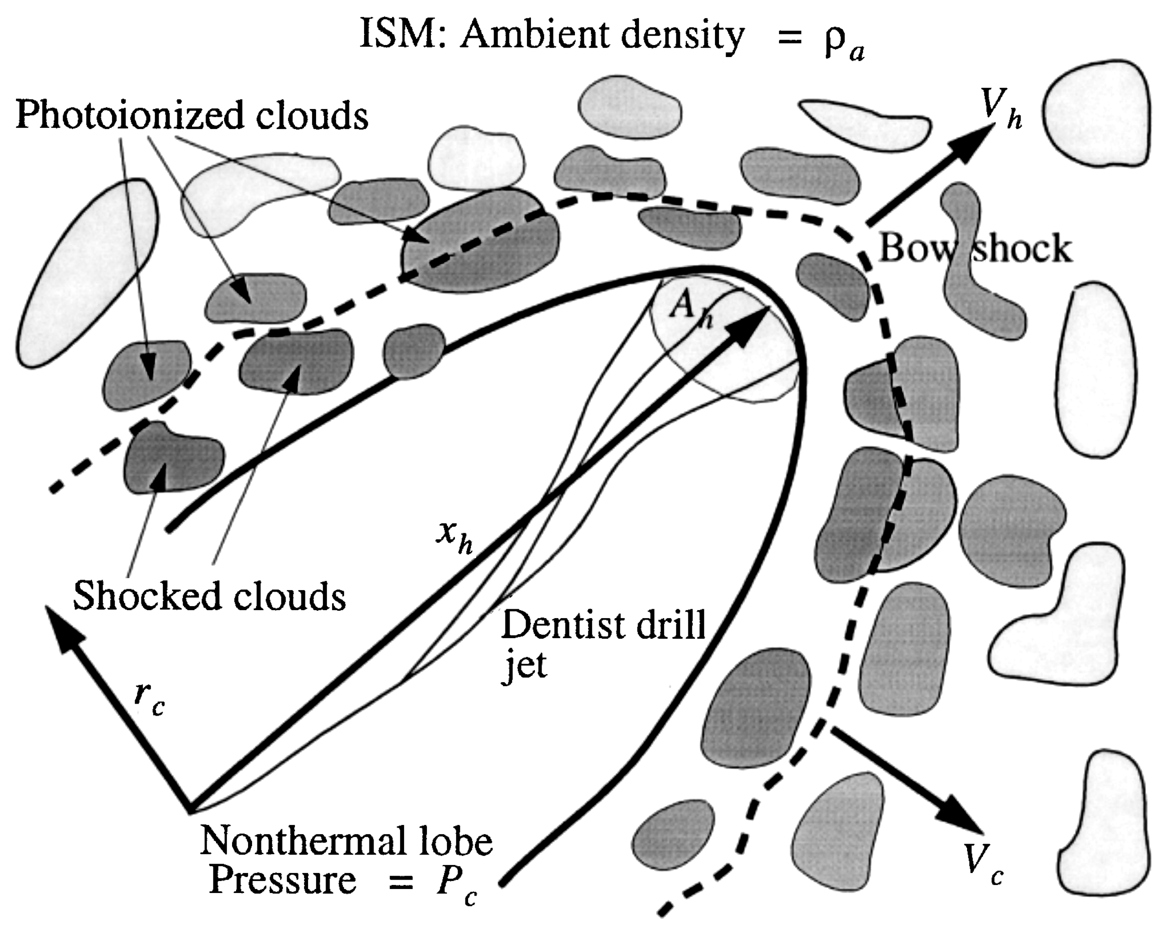

FIG. 1.—Illustration of the interaction of a jet-fed radio lobe with the dense interstellar medium. The radiative bow shock (*dashed line*) surrounding the radio lobe collisionally excites the ISM which is shown here as a two-phase medium permeated by dense clouds shown in light gray. The radiation from the shock also photoionizes clouds (*medium gray*) in the ISM in advance of the bow shock. The shocked clouds are shown as dark gray. When the ionized gas enveloping the radio lobe is sufficiently dense it can free-free absorb the radio emission at GHz frequencies. The ionized medium also forms a Faraday screen which depolarizes the radio emission.

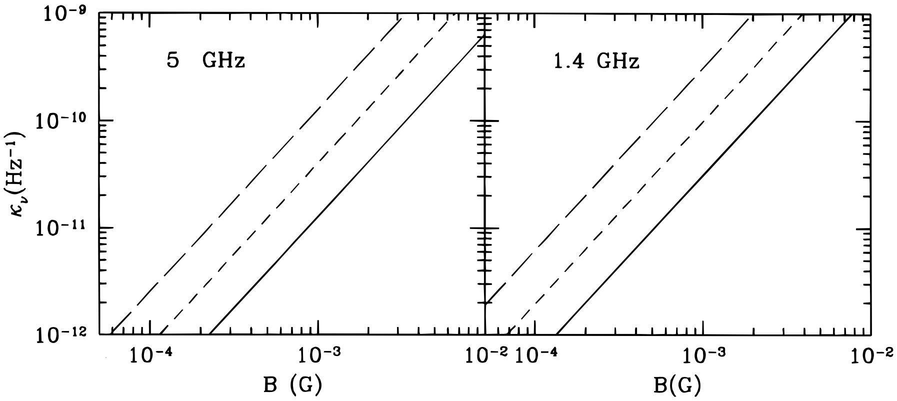

FIG. 2.—Ratio κ_ν of monochromatic radio power to jet energy flux as a function of the magnetic field for a spectral index of 0.7, a lower cutoff Lorentz factor, $\gamma_0 = 1$, and the age parameter $f_e f_{\rm ad} t = 10^5$ yr (*solid lines*), $10^{5.5}$ yr (*short-dashed lines*), and 10^6 yr (*long dashed lines*).

ambient density parameter, ρ_0. Expressing ρ_0 and F_E in terms of ξ and P_0 gives

$$F_E = \frac{2\pi(8-\delta)}{(5-\delta)} \frac{P_0 x_0^3}{t} \xi , \tag{2.8}$$

$$\rho_0 = \frac{\zeta(5-\delta)^2}{9} P_0 \left(\frac{x_0}{t}\right)^{-2} . \tag{2.9}$$

A dynamical age $\sim 10^6$ yr seems relevant for these sources: if their ages were much shorter, we would probably see very few. An age $\lesssim 10^6$ yr is also implied by the model of Begelman (1996) which takes luminosity-size evolution into account.

Typical sizes of GPS sources are ~ 350 pc and typical pressures are $\sim 10^{-6}$ dyne cm^{-2}. To attain these sizes in a timescale of t_6 Myr implies that $\xi \sim 1$ for $x_0 = 350$ pc[5]; this gives (for $\delta = 2$) $F_E \sim 5 \times 10^{44} t_6^{-1}$ ergs s^{-1}, and the hydrogen number density at 350 pc is $730 t_6^2$ cm^{-3}, translating to a number density at 1 kpc of 90 cm^{-3}. We show in subsequent sections that these estimates are reasonably indicative. However, better agreement with parameters in the following sections is obtained if the typical age is slightly less than 1 Myr.

2.3. *Velocity of Advance as a Function of Distance*

The above solution implies that the velocity of advance of the sides of the cocoon, $\zeta^{-1/2} dx_h/dt$ as a function of the distance of the head of the cocoon from the nucleus, x_h, is given by

$$V_c = V_0 \left(\frac{x_h}{x_0}\right)^{[(\delta-2)/3]} , \tag{2.10}$$

where

$$V_0 = \frac{3}{[18(8-\delta)\pi]^{1/3}} \zeta^{1/6} \left(\frac{F_E}{\rho_0 x_0^2}\right)^{1/3} \tag{2.11}$$

$$= 1500 \text{ km s}^{-1} \left(\frac{6}{8-\delta}\right)^{1/3} \zeta^{1/6} \left[\frac{F_{E,45}}{n_{\rm H,0}}\right]^{1/3} , \tag{2.12}$$

$F_{E,45}$ is the energy flux in units of 10^{45} ergs s^{-1}, and n_0 is the hydrogen number density at 1 kpc. Note that for $\delta = 2$ (the upper end of the range favored by Begelman) the shock velocity is independent of the size of the lobe.

[5] Note that we have chosen $x_0 = 350$ pc here for convenience. In the ensuing treatment we refer number densities and scales to $x_0 = 1$ kpc.

Another implication of the above model is that the work done by the expanding cocoon on the ambient medium is

$$P_c \frac{dV}{dt} = \frac{3}{8-\delta} F_E . \tag{2.13}$$

For $\delta = 2$ this amounts to 0.5 F_E. This relation is used in § 4 to evaluate the emission-line luminosities.

2.4. *Jet Energy Flux and Radio Power*

The above expressions for hot-spot distance, pressure, velocity, etc., all involve the jet energy flux which we have estimated above to be of order 10^{45} ergs s^{-1}. Since the median power at 5 GHz of GPS sources in the Stanghellini et al. (1996b) sample is $10^{27.5}$ W Hz^{-1}, the implied ratio of monochromatic power to jet energy flux $\sim 10^{-10.5}$. It is important to determine whether this is consistent with the energy budget of GPS sources, and this, in turn, is useful when we come to examine the relationship between emission-line luminosity and monochromatic radio power in § 4.

In considering the energy budget, we take E_L to be the total lobe energy, f_e to be the fraction of the internal energy in electrons and positrons, B the lobe magnetic field, t the age of the source, and γ_0 the lower cutoff in the electron Lorentz factor distribution. For the above dynamical model, $E_L = f_{\rm ad} F_E t$, where the adiabatic factor is $f_{\rm ad} = (5-\delta)/(8-\delta)$. Expressing the synchrotron emissivity (integrated over 4π solid angle) in terms of the electron pressure, one obtains for the ratio of monochromatic synchrotron power P_ν to energy flux:

$$\kappa_\nu = \frac{P_\nu}{F_E} \approx 4\pi(a-2) c_5(a) c_9(a) f_e f_{\rm ad} \times (\gamma_0 m_e c^2)^{a-2} B^{(a+1)/2} \left(\frac{\nu}{2c_1}\right)^{-\alpha} t , \tag{2.14}$$

where the c_i are the synchrotron parameters defined by Pacholczyck (1970) and the electron distribution $N(E) \propto E^{-a}$. In this expression, κ_ν depends mainly upon the magnetic field, B, and the age, t. For the generic parameters for GPS sources quoted earlier ($p \sim 10^{-6}$ dyne cm^{-2} and $t \lesssim 10^6$ yr) the equipartition magnetic field, $B_{\rm eq} \sim 4 \times 10^{-3}$ G. Hence, values of κ_ν for $\nu = 1.4$ and 5 GHz are plotted in Figure 2 for $\gamma_0 = 1$, $10^{-4} < B < 10^{-2}$, and $f_e f_{\rm ad} t = 10^5$, $10^{5.5}$, and 10^6 yr. It is evident from these plots that a magnetic field of the above order of magnitude, or perhaps slightly less, is consistent with $\kappa_5 \approx 10^{-10.5}$ provided that f_e is not too much less than unity and the age is not too much less than 10^6 yr. The magnetic field *may* be less than its equipartition value for the following reasons: in the evolving lobe, a tangled magnetic field behaves like a relativistic gas. Therefore, the magnetic pressure should approximately track the particle pressure. Assuming that most of the kinetic energy dissipated at the jet shock goes into relativistic particles, the flux of particle energy into the lobe is of order the kinetic energy flux of the jet. On the other hand, the flux of magnetic energy into the lobe is approximately equal to the magnetic energy flux in the jet and is correspondingly less than the particle energy flux by a factor of order the Alfvén number of the jet. Dynamo action may amplify the field to near equipartition; however, it remains to be demonstrated that a dynamo would work in this situation. Moreover, in the case of kiloparsec scale FR2s which are morphologically similar to the sources studied here, simulations (Clarke 1996) show that the observed filamentation depends upon the magnetic energy density being less than the particle pressure. Blandford (1996) has also argued that the magnetic field in Cygnus A is subequipartition on account of the small-scale ordering of the polarization. On the other hand, the necessity for a subequipartition magnetic field decreases if $f_e f_{\rm ad} \ll 1$.

A value of $\kappa_\nu \sim 10^{-10.5}$ is about 1 order of magnitude higher than what one normally takes for large-scale radio sources. For example, such a value implies that a lobe fed by a 10^{43} ergs s^{-1} jet (normally considered to be borderline FR1/2) would have a power $\sim 10^{25.5}$ W Hz^{-1}, about 1 order of magnitude higher than the FR1/2 break. This apparent discrepancy is consistent with the luminosity-size evolution discussed by Begelman (1996), which, as he showed, is implied by the evolutionary dependence of the quantity $B^{(\alpha+1)/2}\, t$ in equation (2.14) above. (For example, for a spectral index $\alpha = 0.7$, $\kappa_\nu \propto t^{-0.7}$.)

We conclude, therefore, that values of $\kappa_\nu \sim 10^{-10.5}$ can be consistent with the energy budget of the classes of radio source we are considering here. However, given the uncertainties in the above calculation and the simplicity of an homogeneous model, variations from this value by up to 1 order of magnitude are to be expected.

3. CONDITIONS FOR RADIATIVE SHOCKS

As the radio lobe pushes its way out through the dense interstellar medium close to the nucleus, a strong shock is driven into this medium. Provided that the shock can become radiative within an evolutionary timescale, then cooling losses supply a powerful source of EUV photons that is available both to pre-ionize an extensive precursor H II region and support a high emission measure recombination region in the shock. Both of these ionized regions can then contribute to the free-free absorption of the nonthermal emission from within the lobes. From detailed models of fast radiative shocks with solar abundance and velocities in the range 500–1000 km s^{-1}, we find that they become radiative and cool to the recombination temperature of hydrogen in a timescale $t_{\rm rad,6}$ Myr, where

$$t_{\rm rad,6} \approx 1.9\, n^{-1} V_3^{2.9}\ ; \tag{3.1}$$

V_3 is the shock velocity velocity in units of 1000 km s^{-1}, and n cm^{-3} is the hydrogen particle density.

In order that the shock be radiative we require the cooling time to be less than a dynamical time, i.e., $t_{\rm rad}/t \lesssim 1$. Since $n = n_0(x/x_0)^{-\delta}$, using equation (2.4) for the distance of the hot spot from the center of the galaxy together with the following equation for the hot spot velocity,

$$v_h = \frac{3}{5-\delta}\frac{x_0}{t}\,\zeta^{(1/5-\delta)}\ , \tag{3.2}$$

gives for the ratio of cooling time to elapsed time

$$\frac{t_{\rm rad}}{t} = 1.7\left(\frac{3}{5-\delta}\right)^{2.9} n_0^{-1}\chi^{[(\delta+2.9)]/(5-\delta)]} t_6^{[(6.9\delta-10.8)/(5-\delta)]}\ , \tag{3.3}$$

where t_6 is the source age in Myr and

$$\chi = \frac{(5-\delta)^3}{18\pi(8-\delta)}\left(\frac{\zeta^2 F_E}{\rho_0 x_0^5}\right)(10^6\ {\rm yr})^3 = 0.85\frac{(5-\delta)^3}{8-\delta}\left(\frac{\zeta^2 F_{E,45}}{n_0}\right). \tag{3.4}$$

For $\delta = 2$,

$$\left(\frac{t_c}{t}\right) \approx 15(\zeta^2 F_{E,45})^{1.63} n_0^{-2.63} t_6\ . \tag{3.5}$$

This equation shows the consistency of our inference of a fairly high density environment for these sources. For jet fluxes $\sim 10^{45.5}$ ergs s^{-1} and normal ISM densities with $n \sim 1$ cm^{-3} would mean that the shock would be nonradiative on timescales $\lesssim 10^5$ yr. When $n_0 \sim 10$–100, the shock at the head of the lobe is radiative up to ages $\sim 10^6$ yr, and this seems appropriate for these sources.

Note also that the above value of t_c/t has been calculated for the shock in advance of the hot spot. This is a factor of $\zeta^{1/2}$ faster than the wall shock at the sides of the cocoon so that the cooling timescale is a factor of $\zeta^{1.44} \approx 2.7$ longer. Therefore, when the head shock becomes nonradiative, the wall shock remains radiative for approximately 1.7 times longer and most of the optical line emission emanates from the sides of the source. That is, an "ionization cone" has been produced.

The fact that the wall shocks are radiative early in the expansion of the bubble while the ambient density is high ensures that the emission measure of the shocked gas and its precursor are also high. Since the radio-free-free opacity depends essentially upon the emission measure, it is feasible that the shocked interstellar medium provides the required free-free opacity in these sources. This is addressed further in § 5.

4. RELATIONSHIP BETWEEN EMISSION-LINE LUMINOSITY AND RADIO POWER

4.1. *Estimates of* Hβ *and* [O III] *Emission-Line Luminosities*

The expansion work done on the interstellar medium is mediated by the shock that precedes the advance of the nonthermal lobe into the surrounding dense gas. In the case that this shock is fully radiative, the total shock luminosity, L_T, and the Hβ and [O III] λ5007 line luminosities ($L_{{\rm H}\beta}$ and L([O III]) resulting from a shock of velocity $V_{\rm sh}$ and area $A_{\rm sh}$ into a medium with unshocked hydrogen density $n_{\rm H}$ are (following Dopita & Sutherland 1996):

$$L_T = 1.14\ V_3^3\left(\frac{n_{\rm H}}{{\rm cm}^{-3}}\right)\left(\frac{A_{\rm sh}}{{\rm cm}^2}\right)\ {\rm ergs\ s^{-1}}\ , \tag{4.1}$$

$$L_{\mathrm{H}\beta} = 1.91 \times 10^{-3}\, V_3^{2.41}\left(\frac{n_{\mathrm{H}}}{\mathrm{cm}^{-3}}\right)\left(\frac{A_{\mathrm{sh}}}{\mathrm{cm}^2}\right) \text{ ergs s}^{-1}\,, \tag{4.2}$$

$$L([\mathrm{O\,III}]) = 2.3 \times 10^{-2}\, V_3^{3}\left(\frac{n_{\mathrm{H}}}{\mathrm{cm}^{-3}}\right)\left(\frac{A_{\mathrm{sh}}}{\mathrm{cm}^2}\right) \text{ ergs s}^{-1}\,, \tag{4.3}$$

where V_3 is the shock velocity in units of 1000 km s^{-1}. Since the shock luminosity is equal to the rate of work done by the expansion of the lobe, i.e.,

$$L_T = \frac{3}{8-\delta} F_E\,, \tag{4.4}$$

it follows that

$$L(\mathrm{H}\beta) = 8.5 \times 10^{-4}\left(\frac{6}{8-\delta}\right) V_3^{-0.59} F_E \text{ ergs s}^{-1}\,, \tag{4.5}$$

$$L([\mathrm{O\,III}]) = 1.0 \times 10^{-2}\left(\frac{6}{8-\delta}\right) F_E \text{ ergs s}^{-1}\,. \tag{4.6}$$

Since the [O III] and total line luminosities depend upon the same power of the shock velocity, the velocity dependence cancels out in the final expression relating L([O III]) to energy flux. However, there is a weak dependence of Hβ luminosity upon shock velocity. Since the lobe (and shock) areas are dominated by the sides of the cocoon, we therefore use the cocoon velocity given by equation (2.10) to estimate L(Hβ), with the result that

$$\begin{aligned} L(\mathrm{H}\beta) &= 6.7 \times 10^{41}\, \zeta^{-0.098}\left(\frac{6}{8-\delta}\right)^{0.80} F_{E,45}^{0.80}\, n_{\mathrm{H},0}^{0.20} \\ &\quad \times \left(\frac{x_h}{x_0}\right)^{-0.20(\delta-2)} \text{ ergs s}^{-1} \\ &= 6.7 \times 10^{41}\, \zeta^{-0.098}\left(\frac{6}{8-\delta}\right)^{0.80} n_{\mathrm{H},0}^{0.20}\left(\frac{\kappa_{1.4}}{10^{-11}}\right)^{-0.80} \\ &\quad \times \left(\frac{P_{1.4}}{10^{27}\text{ W Hz}^{-1}}\right)^{0.80}\left(\frac{x_h}{x_0}\right)^{-0.20(\delta-2)} \text{ ergs s}^{-1}\,, \end{aligned} \tag{4.7}$$

where $P_{1.4}$ is the monochromatic radio power at 1.4 GHz and κ_ν is the conversion factor from jet energy flux to monochromatic radio power as discussed in § 2. This relationship shows a very weak dependence on the scaling density n_0 and the size of the source, x_h. The Hβ luminosity is independent of size for $\delta = 2$.

The [O III] luminosity in terms of jet energy flux and radio power is

$$\begin{aligned} L([\mathrm{O\,III}]) &= 1.0 \times 10^{43}\left(\frac{6}{8-\delta}\right) F_{E,45} \text{ ergs s}^{-1} \\ &= 1.0 \times 10^{43}\left(\frac{6}{8-\delta}\right)\left(\frac{\kappa_{1.4}}{10^{-11}}\right)^{-1} \\ &\quad \times \left(\frac{P_\nu}{10^{27}\text{ W Hz}^{-1}}\right) \text{ ergs s}^{-1}\,. \end{aligned} \tag{4.8}$$

For the purpose of comparison with the observational data presented by (Gelderman & Whittle 1996, hereafter GW) we also give here the theoretical Hα + [N II] luminosity. MAPPINGS models of 500–1000 km s^{-1} shocks show that the ratio of Hα + [N II] to Hβ luminosities is approximately constant at 5.2 ± 0.2. Hence equation (4.2),

$$\begin{aligned} L(\mathrm{H}\alpha + [\mathrm{N\,II}]) &= 4.0 \times 10^{42}\, \zeta^{-0.098}\left(\frac{6}{8-\delta}\right)^{0.80} \\ &\quad \times n_{\mathrm{H},0}^{0.20}\left(\frac{\kappa_{1.4}}{10^{-11}}\right)^{-0.80}\left(\frac{P_{1.4}}{10^{27}\text{ W Hz}^{-1}}\right)^{0.80} \\ &\quad \times \left(\frac{x_h}{x_0}\right)^{-0.20(\delta-2)} \text{ ergs s}^{-1} \end{aligned} \tag{4.9}$$

4.2. *Comparison with Observational Data*

4.2.1. [O III] *Luminosity*

GW in their study of the optical properties of CSS sources have determined the luminosities of a number of spectral lines, including [O III] λ5007 and Hα + [N II]. Combining data relating to radio galaxies, radio loud quasars, CSS radio galaxies, and CSS quasars, they have demonstrated the existence of correlations (albeit with some scatter) between emission-line fluxes and monochromatic radio power over about 5 decades in either parameter. The CSS sources fit neatly into the high-power end of this correlation. Tadhunter et al. (1993) and Morganti, Killeen, & Tadhunter (1993) (referred to hereafter as TM) have also obtained [O III] luminosities and radio powers for the Wall & Peacock (1985) sample. These relate principally to extended radio sources. However, there are a number of unresolved sources in this sample which have subsequently been shown to be CSS sources (Morganti 1996, private communication). Therefore, we have combined the two samples in order to increase the statistics. Moreover, it is of interest to compare the relation between radio and optical emission for the compact and extended sources.

Thus, in Figure 3 we present the [O III]λ5007/1.4 GHz radio data from these two samples with theoretical predictions, derived from equation (4), overlaid on the data. In view of the unavoidable uncertainty in the parameter $\kappa_{1.4}$ (see § 2) theoretical lines are drawn for $\kappa_{1.4} = 10^{-10.5}$, 10^{-11}, and $10^{-11.5}$, respectively.

It is evident from Figure 3 that the theoretical lines bracket most of the data for the high-power ($P_{1.4} \gtrsim 10^{25.5}$ W Hz^{-1}) sources. However, there are some intriguing features to the diagram. The first is that the CSS sources (*filled symbols*) lie to the right of the mean correlation. A mean value of $\kappa_{1.4} \approx 10^{-10.5}$ seems most appropriate. On the other hand, the quasars (*crosses*) lie to the left with an appropriate mean $\kappa_{1.4} \approx 10^{-11}$. This may be a result of an extra source of ionization in the quasars or it may imply more efficient production of radio emission in the CSS sources. The second feature is that for $P_{1.4} \lesssim 10^{25.5}$ W Hz^{-1}, the [O III] luminosities of the radio galaxies (*open symbols*) are, on average, about 1 order of magnitude less than implied by the theoretical lines and any sensible value of $\kappa_{1.4}$. Our interpretation of this feature is that these (presumably borderline FR1/2) galaxies represent those in which the bow shock has ceased to be radiative and has broken out of the dense environment surrounding the nucleus (see § 3). In this case, the conversion of jet energy flux into [O III] emission appears to be considerably less efficient (about 5%) and may occur, for example, through the interaction of the jets with dense clouds in the galaxy

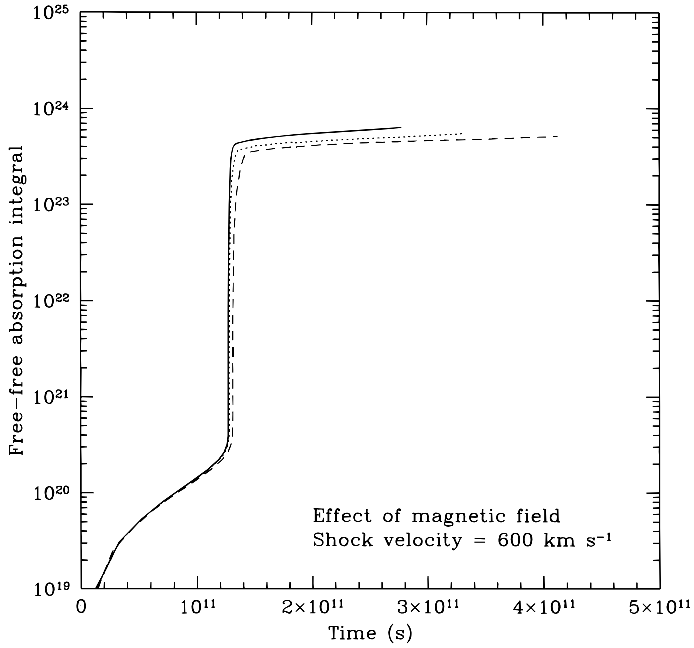

FIG. 3.—Contribution to the optical depth parameter $\int n_e^2 T_4^{-1.35} dl$ from different temporal regions of the postshock gas for a shock velocity of 600 km s^{-1}. They are parameterized by the magnetic parameter, $Bn^{-1/2}$ (in units of μG cm$^{3/2}$). *Solid line*, $Bn^{-1/2} = 2$; *dotted line*, $Bn^{-1/2} = 4$; *dashed line*, $Bn^{-1/2} = 8$. Note that the dominant contribution to the integral is from the recombination/cooling zone, the beginning of which is marked by the point where the curves abruptly steepen.

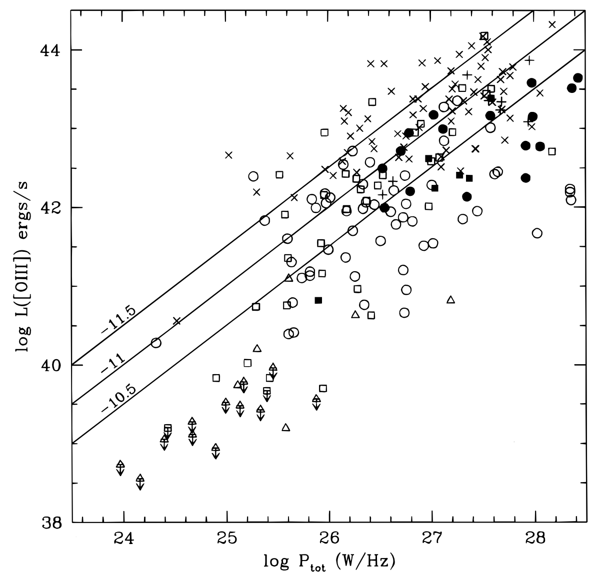

FIG. 4.—Predicted [O III] luminosity as a function of radio power for three values of the parameter log $\kappa_{1.4} = -10.5$, -11.0, and -11.5 overlaid on data for extragalactic radio sources. *Filled circles*, CSS sources from GW; *filled squares*, CSS sources from TM; *open circles*, GW FR2 radio galaxies; *open squares*, TM FR2 radio galaxies; *crosses*, GW QSOs; *plus signs*, TM compact flat spectrum sources; *open triangles*, TM FR1 radio galaxies. Upper limits are indicated in the usual way.

(e.g., Sutherland, Bicknell, & Dopita 1993) but not with a single large confining dense cloud as we have invoked for the GPS/CSS sources. These speculations could be settled by a morphological comparison of the emission-line luminosity from sources in the various parts of the diagram.

4.2.2. [Hα] + [N II]

Figure 4 shows the theoretical lines for the Hα + [N II] luminosity overlaid on the observational data for CSS radio galaxies, radio galaxies and "other" radio galaxies from (Gelderman & Whittle 1996). The predicted line flux depends upon the density in a minor fashion, and the theoretical lines correspond to a scaling density of $n_0 = 10$ cm^{-3}. Again, the theoretical lines bracket a large part of the data, and the small number (4) of CSS sources lie to one side of the correlation and appear to be best fit by $\kappa_{1.4} \approx 10^{-10.5}$. Without a corresponding data set to that of TM, the dropoff of radio galaxies from the general correlation at $P_{1.4} \approx 10^{25.5}$ W Hz^{-1} is not evident. Nevertheless, there is still a group of radio galaxies to the right of the line defined by $\kappa_{1.4} = 10^{-10.5}$ which could represent a less efficient conversion of jet energy to Hα + [N II] luminosity.

Note that there is greater scatter in the [O III] diagram compared to that in the Hα + [N II] diagram. This is probably the result of reddening. Indeed Baker & Hunstead (1996) have argued that the CSS sources in the Molonglo quasar sample are substantially reddened ($A_V \approx 4$) because of the large Balmer decrement. Given that the [O III] fluxes are affected by absorption, it is not necessary to assume as large a radiative efficency, $\kappa_{1.4}$, as has been assumed above.

5. FREE-FREE ABSORPTION OF THE RADIO EMISSION

5.1. *Free-Free Absorption by Shocked and Precursor Gas*

In our model, the radio lobe is surrounded by fast radiative shocks. Such shocks have very high emission measure both in their photoionized precursors and in their recombination/cooling zones, as established in the previous section. This gives rise to free-free absorption of the radio emission. The free-free optical depth at radio wavelengths is given by

$$\tau_\nu = 1.1 \times 10^{-25} \nu_9^{-2.1} \int n_e^2 T_4^{-1.35} dl , \quad (5.1)$$

where ν_9 is the frequency in GHz and T_4 is the electron temperature in units of 10^4 K (Lang 1980). We have used steady-flow, plane-parallel shock models to establish values of the integral in the above equation.

In principal, the integrals of $n_e^2 T_4^{-1.35}$ through the shock and precursor regions depend on the adopted value of the magnetic parameter $Bn^{-1/2}$. However, the dependence upon this parameter is weak, as shown in Figure 5. Note also that Figure 5 shows that, in the shock region, by far the largest contribution to the integral comes not from the postshock cooling flow, but from the photoionized layer in the recombination zone of the shock (as a result of the dependence on the temperature). These shock models show that, for steady state, one-dimensional shocks viewed at normal incidence:

$$\int n_e^2 T_4^{-1.35} dl = 1.78 \times 10^{22} V_3^{2.3} n(\mathrm{H}) \quad (\text{shock}) ,$$
$$= 9.06 \times 10^{21} V_3^{1.5} n(\mathrm{H}) \quad (\text{precursor}) , \quad (5.2)$$

where V_3 is the shock velocity in units of a thousand km s^{-1}. (These expressions are for values of $B/n^{1/2} = 4$ μG

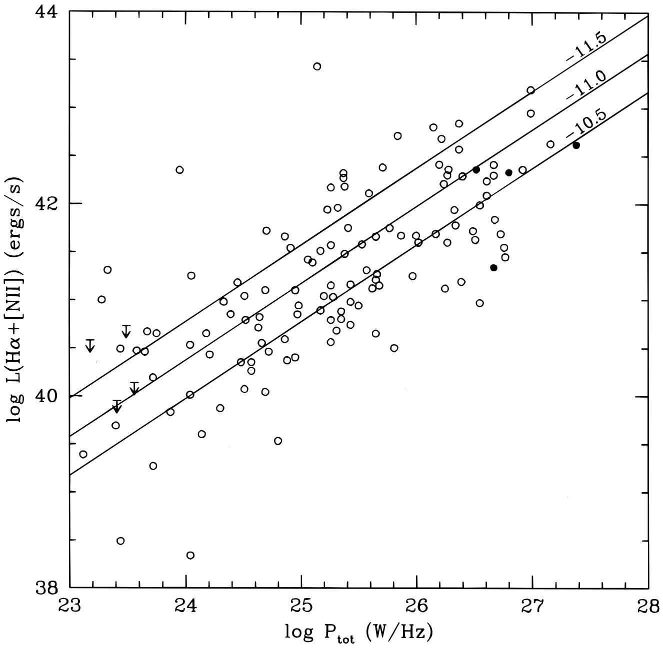

FIG. 5.—Predicted Hα + [N II] luminosity as a function of radio power at 1.4 GHz for three values of the parameter log $\kappa_{1.4} = -10.5$, -11.0, and -11.5 overlaid on data for extragalactic radio sources. The filled and open circles, represent respectively, GW CSS radio galaxies and normal radio galaxies.

cm$^{3/2}$.) The integral through the shock is somewhat greater than the integral through the precursor mainly because of the lower temperature that is encountered in the photoabsorption/recombination zone of the shock. These equations imply that free-free absorption by a 1000 km s^{-1} shock could produce a GHz peak source provided that the preshock hydrogen density, n(H), is of order 100 cm^{-3}. In this case the radiative shock thickness is ~ 3 pc, and the total thickness of the photoionized precursor is ~ 100 pc. These parameters are quite consistent with those derived in previous sections and imply that the ionized gas is typically confined to a relatively thin shell around the nonthermally emitting lobes of typical GPS sources the sizes of which range from about 100 pc to 3 kpc (Fanti et al. 1990; Stranghellini et al. 1996a).

One-dimensional models are an approximation because, as we show below, the interpretation of the spectra of GPS and CSS sources probably require that some regions of the source be broken up into a number of clouds and/or filaments. Nevertheless, we use the integrated emission measure from the MAPPINGS output to approximate the mean optical depths in the different shock regions and also to establish the scaling relations with shock velocity. We return to this point after discussing the shape of the GPS spectra.

5.2. *Absorption from an Ensemble of Clouds*

The catalog of spectra by Stanghellini et al. (1996b) provide a strong constraint on the nature of the absorbing region. In particular, the low-frequency spectrum, in both radio galaxies and quasars, is usually well fitted by a power law with a mean spectral index ~ -1 ($F_\nu \propto \nu^{-\alpha}$). This is especially evident in the (usually small) sources whose turnover is in the tens of GHz range, so that the low-frequency end of the spectrum is well sampled.

If the radio spectrum were absorbed by a uniform screen of ionized plasma, the spectrum would behave as $\exp(-a\nu^{-2.1})$ at low frequencies, inconsistent with the observed spectra. We therefore model the spectrum as the result of the absorption of a nonthermal power law by clouds with a range of optical depths. There are two possible origins for such a structure. (1) The medium surrounding the source exists in two phases. This would give spatially variable absorption in both the precursor and shocked gas. Such clouds would also be shredded by the passage of the fast shocks adding extra structure to the absorbing screen. (2) The postshock gas is thermally unstable. Thus, even in the case of a uniform external medium it will develop a porous screen of clouds and filaments in the photoionization/recombination region of the postshock flow. Since the optical depths through the postshock region and the precursor region are comparable, both of these regions are required to exhibit a range of optical depths in order to account for the low-frequency power law.

The investigation of both of the above scenarios constitute an interesting exercise in the computational astrophysics of radiative shocks beyond the scope of this paper. Nevertheless, *some* insight into the second case can be obtained by the following argument. Let us consider the fate of an inhomogeneity in the postshock flow and compare its resultant surface area in the recombination region to the surface area that would result in the strictly one-dimensional, unperturbed case. Treating the perturbed flow as a quasi-one-dimensional steady flow, then mass conservation implies that the density, ρ_{rec}, velocity, v_{rec}, and surface area, A_{rec} of the cloud in the recombination region satisfy $\rho_{rec} v_{rec} A_{rec} \approx F_M$, where F_M is the mass flux through the initial area of the shock. Now the density in the recombination zone is determined by the approximately isobaric shock pressure and the recombination temperature; the velocity is determined by the energy equation and is approximately independent of the perturbation. Hence the surface area of the perturbed cloud is approximately equal to that which would hold in the unperturbed cloud. Moreover, if we trace the mass of gas which eventually makes up the recombination region of the flow, then since this is conserved, inhomogeneities which result in a smaller surface area (than the one-dimensional case) will have a larger transverse size and a larger optical depth and conversely for inhomogeneities which result in a larger surface area. Thus the effect of postshock thermal instabilities is likely to be a range of optical depths through the postshock gas.

We also expect that gas which has been shredded in shocks should also show a distribution of optical depths. Nevertheless, the details of optical depth variations in these circumstances clearly requires further investigation. The spectral model developed below serves to outline the type of optical depth variation that is necessary in order to explain GPS and CSS spectra.

5.3. *A Spectral Model*

5.3.1. *The Spectrum Resulting from a Distribution of Optical Depths*

The specific intensity of a ray passing from the radio lobe through the absorbing screen is

$$I_\nu = A_\nu^{-\alpha} \exp(-a\nu^{-2.1}), \tag{5.3}$$

where A characterizes the amplitude of the incident synchrotron spectrum, α is the spectral index, and, as described above, $a \propto \int n_e^2 T_4^{-1.35} dl$. Since we do not have a comprehensive theory for the distribution of optical depths in the absorbing clouds, we allow for a range of values of the parameter a via a power-law distribution $\propto a^p$, where $p > -1$ and a varies between 0 and a maximum value a_0. In the light of the above discussion we do not expect the power law to be too steep, i.e., the index p should be reasonably close to zero. We further assume that the amplitude, A, of the incident synchrotron spectrum varies more slowly over the face of the lobe than the variation of the absorption parameter, a (i.e., the length scale of the shock and/or ISM inhomogeneities is much less than the size of the lobe) then the average value of I_ν is given by

$$\langle I_\nu \rangle = A \frac{p+1}{a_0^p} \int_0^{a_0} \exp(-a\nu^{-2.1}) a^p \, da \tag{5.4}$$

$$= A(p+1)\left(\frac{\nu}{\nu_0}\right)^{2.1(p+1)-\alpha} \int_0^{(\nu/\nu_0)^{-2.1}} u^p e^{-u} \, du \tag{5.5}$$

$$= A(p+1)\left(\frac{\nu}{\nu_0}\right)^{2.1(p+1)-\alpha} \gamma\left[p+1, \left(\frac{\nu}{\nu_0}\right)^{-2.1}\right], \tag{5.6}$$

where we have defined the characteristic frequency ν_0 by $a_0 = \nu_0^{2.1}$ and

$$\gamma(p+1, x) = \int_0^x u^p \exp(-u) du$$

is the incomplete gamma function of order $p + 1$. A factor of ν_0^α has been absorbed into A. It is straightforward to show that the low- and high-frequency limits of equation (5.6) are given by

$$\langle I_\nu \rangle = A\Gamma(p+2)\left(\frac{\nu}{\nu_0}\right)^{2.1(p+1)-\alpha}, \quad \nu \ll \nu_0 ;$$

$$= A\left(\frac{\nu}{\nu_0}\right)^{-\alpha}, \quad \nu \gg \nu_0 . \tag{5.7}$$

Hence, the low-frequency spectral index, α_l, is given by

$$\alpha_l = \alpha - 2.1(p+1) , \tag{5.8}$$

and the inferred value of p, characterizing the distribution of absorbing clouds is

$$p = \frac{\alpha - \alpha_l}{2.1} - 1 . \tag{5.9}$$

If the parameter a_0 (equivalently, the frequency ν_0), describing the maximum value of the absorption by the ensemble of clouds does not vary significantly over the area of the lobe, then equation (5.6) with I_ν replaced by the monochromatic power P_ν should provide an adequate representation of the source spectrum. The variation of the line of sight over the lobe is a geometrical factor that could give rise to significant variation of ν_0. Variation in the local shock velocity, to which the optical depth is quite sensitive, is another factor which could lead to significant variation of ν_0. The major effect on the spectrum of a variation of ν_0, with p remaining constant, would be a broadening of the spectral peak but with the same asymptotic low- and high-frequency slopes.

Examples of the fit of the above spectrum to three sources in the Stanghellini et al. (1996b) sample are shown in Figure 6, and the parameters of the fits are given in Table 1. Since, in each case, the fit involves four parameters and approximately 10 data points, these fits cannot be taken as compelling evidence that this form of spectrum is correct. However, it is reassuring that a comparatively simple and analytical expression should provide such an excellent fit to the data.

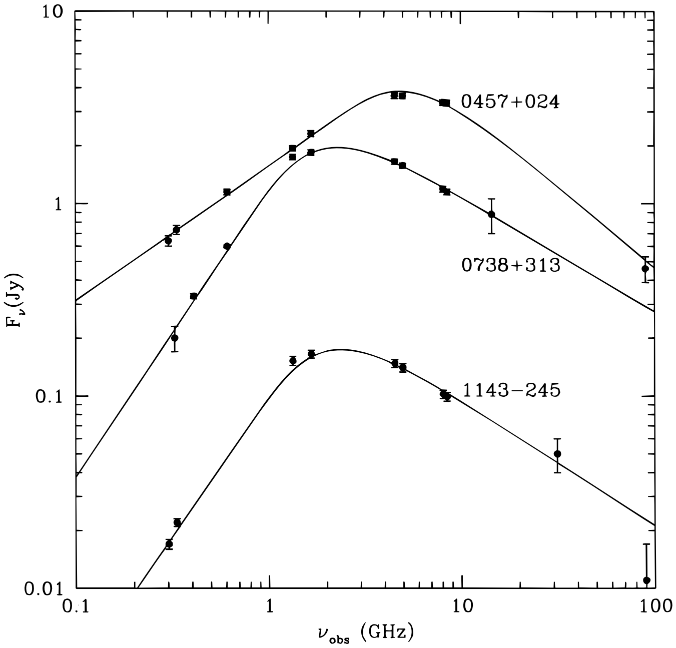

FIG. 6.—Fits of the model spectrum to three sources in the sample of Stanghellini et al. (1996). The spectrum for 1143-245 has been shifted down by a factor of 10 to avoid confusion. The parameters of the fits are given in Table 1.

If the low-frequency power law is the result of absorption in either the shock or precursor component, and if the other component is uniform, then one would expect to see the signature of an exponential cutoff in the spectra. For some of the sources in the Stanghellini et al. (1966b) sample, with turnovers near 1 GHz, the low-frequency coverage is inadequate to say whether this is the case or not. However, in the sources with peaks at higher frequencies, there is no indication of such a signature. This suggests a range of optical depths in both precursor and shocked regions and that the ISM surrounding the source is clumpy and presumably is in a two-phase form. If this deduction is correct there will likely be a contribution to the optical depth from shock shredding of clouds together with associated thermal instabilities.

5.3.2. *The Distribution of the Parameter p*

We have assumed that the spectrum is of the form given by (5.7) and used the Stanghellini et al. (1996b) compilation of low- and high-frequency spectral indices to calculate the

TABLE 1

PARAMETERS OF SPECTRAL FITS

Source	A	ν_0	α	p
0457+024......	3.0	1.85	0.6	0.0
0738+313......	4.1	5.4	0.85	−0.26
1143−245......	2.7	2.0	0.65	0.0

distribution of p implied by our model. The mean value of p is -0.17 and its standard deviation is 0.25, consistent with the above inference of a nearly uniform distribution. It should be noted, however, that the describing the spectrum in this way is possibly an oversimplification. The optical depth distribution in the precursor and postshock regions could well be different since the former is mainly determined by the preexisting distribution of dense clouds and the latter by instabilities. Nevertheless, for the following deductions of turnover frequency versus source size the assumption of a single value of p is not overrestrictive, as is evident below, and the introduction of two values of this parameter is an unwarranted complication at this stage.

One could criticize the assumption of a power-law distribution of optical depths, as being ad hoc. On the other hand, the interpretation of the observed spectra in terms of free-free absorption demands a distribution of optical depths with the general features that we have inferred, i.e., a reasonably broad distribution of the absorption parameter with no particular value of this parameter dominating.

5.4. *Relationship between Turnover Frequency and Size*

We now combine the previous results to show that a theoretical relationship between turnover frequency and source size is readily produced to explain the important observed inverse correlation between these parameters. In terms of our theoretical spectrum, the frequency of the peak in the spectrum depends upon the parameters $\nu_0 = a_0^{1/2.1}$ and p. The ratio of the peak frequency, ν_p, to ν_0 varies in a minor way with p and for the mean value $\bar{p} \approx -0.17$ implied by the data, $\nu_p \approx 1.08 nu_0$. We further assume that the mean value of the absorption parameter, $\langle a \rangle$, is given by the sum of equations (5.2). Since $\langle a \rangle = (p+1)/(p+2)a_0$, then, combining equation (5.1) for the free-free optical depth, equations (5.2) for the optical depths in the shock and precursor regions and inserting the density dependence of the background,

$$\nu_p \approx 1.1\left(\frac{p+2}{p+1}\right)^{0.48} (1.96 \times 10^{-3} V_3^{2.3} + 9.97 \times 10^{-4} V_3^{1.5})^{0.48} \times n_0^{0.48}\left(\frac{x}{\mathrm{kpc}}\right)^{-0.48\delta}, \quad (5.10)$$

with $p \approx -0.17$ and the shock velocity V_3 in units of 1000 km s^{-1} given by the expression in equation (2.10) for the cocoon expansion velocity as a function of distance from the source.

Plots of this relationship for selected parameters compared to the data (Fanti et al. 1990; Stanghellini et al. 1996b; O'Dea & Baum 1996) are shown in Figure 7. Three panels show the predicted relationship between turnover frequency and size for the density power-law index, $\delta = 2$ and three energy fluxes (10^{45}, $10^{45.5}$, and 10^{46} ergs s^{-1}) and n_0, the density at 1 kpc equal to 1, 10, and 100 cm^{-3}. For this value of δ the best fit is provided by $n_0 \approx 10$ cm^{-3}, and the range of jet energy fluxes, which are consistent with the range of radio luminosities, accounts for the spread in the data. The velocities corresponding to the various energy flux and number density parameters are shown in Table 2. It is evident from that table that for energy fluxes $\gtrsim 10^{45}$ ergs s^{-1} and for $n_0 = 1$ cm^{-3}, the shock velocities are too high compared to the observations. Indeed, these shock velocities are beyond the domain of validity of the emission-line models. However, for $\delta = 2$ and $n_0 = 10$–100 cm^{-3}, most of the shock velocities, especially those corresponding to the lower energy fluxes, are consistent with the observations. The same is true for the $\delta = 0.8$, $n_0 = 10$ models when it is taken into account that here the velocity decreases with size as $x^{-0.4}$.

TABLE 2

VELOCITIES CORRESPONDING TO ENERGY FLUX AND NUMBER DENSITY

δ	log F_E (ergs s^{-1})	n_0 (cm^{-3})	V_0 (km s^{-1})
2........	45.0	1	1680
2........	45.5	1	2470
2........	46.0	1	3630
2........	45.0	10	782
2........	45.5	10	1150
2........	46.0	10	1680
2........	45.0	100	363
2........	45.5	100	532
2........	46.0	100	782
0.8......	45.0	10	735
0.8......	45.5	10	1080
0.8......	46.0	10	1580

The presence of the cocoon velocity in equation (5.10) for the turnover frequency means that the dependence on the density parameters δ and n_0 is not as marked as one might initially expect. The first three panels of Figure 7 show the dependence upon density. The dependence upon δ is shown by the lower right-hand panel which corresponds to $\delta = 0.8$ and $n_0 = 10$ cm^{-3}. This provides a better fit to the slope of the data. However, because of the insensitivity of this slope to δ, the best we can say from the fit to the turnover frequency–size relationship alone, is that $\delta \approx 0.8$–2.2, encompassing the range $\delta \approx 1.5$–2 inferred by Begelman (1996) from luminosity-size statistics.

These fits to the turnover-size relation do not depend sensitively on our model for the spectrum. Different assumptions on the spatial distribution of absorbing clouds give a different weighting to the contributions to the optical depth from shock and precursor region. However, as long as the distribution of optical depths around the mean is not wildly skewed, approximately the same expression for the turnover frequency is obtained in all circumstances.

6. POLARIZATION

One of the key features of GPS sources is that they are weakly polarized with typical fractional polarizations $\sim 1\%$ while at the same time exhibiting large rotation measures, typically between 0 and ~ 1000 rad m^{-2} but sometimes as high as several thousand rad m^{-2} (O'Dea et al. 1990; Taylor et al. 1992; Wilkinson et al. 1994; Stanghellini et al. 1996b). This has a natural explanation in terms of our model. The rotation measure through the ionized gas surrounding the lobes is substantial and variations in rotation measure can produce such a large Faraday dispersion that the sources are almost completely depolarized.

There is a contribution to the rotation measure from the magnetic field (approximately interstellar) existing in the

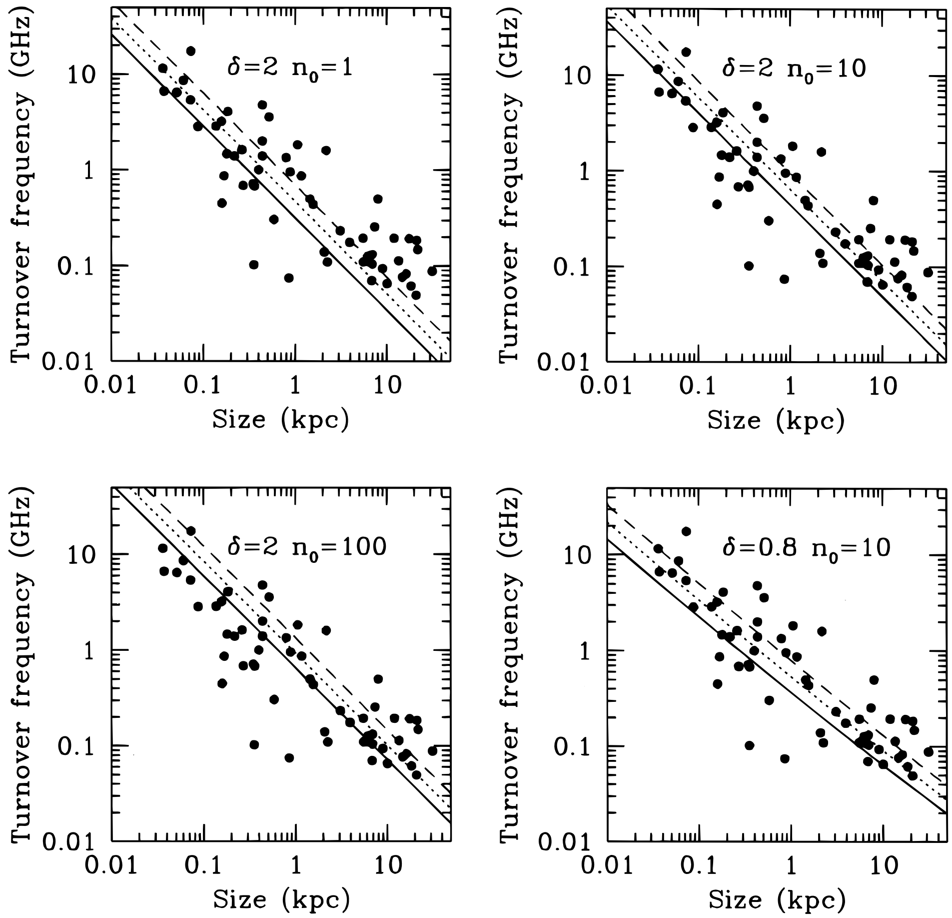

FIG. 7.—Theoretical fits to the turnover frequency vs. size data for GPS and CSS sources. Jet energy fluxes of 10^{45}, $10^{45.5}$, and 10^{46} ergs s^{-1} are represented by solid, dotted, and dashed lines, respectively. Filled dots represent data from Fanti et al. (1990), Stanghellini et al. (1996a), and O'Dea & Baum (1996). Other parameters for the theoretical fits are indicated in each panel.

precursor region and the varying magnetic field existing in the ionized postshock region. In the MAPPINGS shock models, the field is taken to be perpendicular so that $B \propto n_{\rm H}$. Therefore, the quantity $\int n_e B\, dl$ which is required to evaluate the rotation measure along a ray is proportional to $\int n_e n_{\rm H}\, dl$ which is readily estimated from the mappings models. We have for a shock of velocity V_3 thousand km s^{-1}:

$$\int n_e n_{\rm H}\, dl = 9.7 \times 10^{22} V_3^{3.4} n_{\rm H}\ {\rm cm}^{-5} \quad ({\rm shock})\,,$$

$$\int n_e n_{\rm H}\, dl = 2.4 \times 10^{22} V_3^{2.5} n_{\rm H}\ {\rm cm}^{-5} \quad ({\rm precursor})\,. \quad (6.1)$$

Taking the angle between the magnetic field and the line of sight to ψ, the rotation measure, $\phi = 2.5 \times 10^{24} \int n_e B \cos \psi\, dl$ and

$$\phi = 2.5 \times 10^{10} V_3^{3.4} B_{\rm ISM}\ {\rm rad\ m}^{-2} \quad ({\rm shock})\,,$$
$$= 5.7 \times 10^{9} V_3^{2.5} B_{\rm ISM}\ {\rm rad\ m}^{-2} \quad ({\rm precursor})\,. \quad (6.2)$$

For a characteristic interstellar magnetic field $\sim 1 \times n_{\rm H}^{1/2}$ μG and $n_{\rm H} \sim 10$ cm^{-3} and a shock velocity, say ~ 500 km s^{-1}, these equations give rotation measures $\sim 7000 \cos \psi$ and $1500 \cos \psi$ rad m^{-2} for shock and precursor, respectively. These estimates should be indicative of more general magnetic field configurations.

With rotation measures of this order of magnitude and with variation of the rotation measure across the lobe due to field reversals, it is not suprising that GPS and CSS sources are substantially depolarized. Indeed, in order to keep the predicted rotation measure between the observed limits of 0 and 1000 rad m^{-2} (Stanghellini et al. 1996b), it is necessary to invoke a large number ($\sim$10–100) of magnetic field reversals across the source, especially for higher shock velocities. Some field tangling could also be induced by shocks in individual clouds. Hence, a prediction of this theory is that high-resolution VLBI observations should reveal a rich rotation measure structure perhaps similar to that observed in Cygnus A (Dreher, Carilli, & Perley 1987).

7. DISCUSSION AND CONCLUSIONS

In this paper we have proposed a consistent picture of the optical and radio properties of the classes of AGNs variously known as compact symmetric objects, compact steep spectrum sources, and gigahertz peak spectrum sources. This picture unifies the optical and radio properties of these sources in that it shows that the crucial relationship between turnover frequency and size discovered by Stanghellini et al. (1996b), can be explained by free-free absorption by ionized gas produced in radiative shocks surrounding the expanding radio source. Moreover, the predicted relationship between optical line emission and radio power which is a natural consequence of our model agrees well with the data.

The main parameters determining the physics of the radio source–ISM interaction are the energy flux in the jet and the ambient density of the interstellar medium. We have shown that the required energy fluxes are consistent with the level of radio emission provided that the ratio, κ_ν, of monochromatic power to jet energy flux is a factor of a few higher for these compact sources than it is for kiloparsec-scale Fanaroff-Riley class 1 (FR1) and class 2 (FR2) galaxies. This is, in turn, consistent with the luminosity-size evolution proposed by Begelman (1996) and may necessitate a magnetic field strength less than the equipartition value. A value of $\kappa_{1.4} \approx 10^{-10.5}$ gives a good fit to the correlation between radio and emission-line power discovered by Gelderman & Whittle (1996).

We have no independent estimate of the density of the interstellar medium surrounding this class of AGNs. However, we have shown that our favored value for the mean hydrogen density at 1 kpc, $n_0 \approx 10$–$100\ \mathrm{cm}^{-3}$ is consistent with source dynamics (sizes and estimated ages), the condition for radiative shocks to form, and the relationship between the peak radio frequency and source size. In addition, lower and higher values of this parameter give wall shocks which are, respectively, too fast or too slow to be consistent with the observed line widths. The immediate implication of this is that these sources should contain a large amount of cold material. If the matter is spherically distributed, the mass within radius r, $M(r) \approx 4.5 \times 10^8 n_0 (3 - \delta)^{-1} (r/\mathrm{kpc})^{3-\delta} M_\odot$ (for $\delta \leq 2$). For a nonspherical distribution, this estimate is indicative. Hence, if $\delta \approx 1.5$–2, $n_0 \approx 10$, and if the distribution extends to, of order, the size of the largest sources (~ 10 kpc), some 3×10^9–$10^{11}\ M_\odot$ of gas are implicated. This is consistent with the amount of gas which can be fed into the central regions of a galaxy in a merger. It is also qualitatively consistent with the substantial visual absorption, $\langle A_V \rangle \approx 4$, estimated in CSS sources by Baker & Hunstead (1996). We note that the imaging data of Stanghellini et al. (1993) and Gelderman (1994) support the notion that GPS and CSS sources are formed in merging/interacting systems.

The column depth of neutral material is also of interest for the low-frequency cutoff in X-ray observations. This is dominated by the distribution of gas close to the source, and, in estimating it, we exclude the region evacuated of neutral gas by the radio bubble. The column density $n_{\mathrm{col}} \approx n_0 x_0 (\delta - 1)^{-1} (x_h/x_0)^{-(\delta-1)}$. For $n_0 \approx 10\ \mathrm{cm}^{-3}$ and a mean size $x_h \approx 350$ pc, $n_{\mathrm{col}} \sim 10^{23}\ \mathrm{cm}^{-3}$.

We have pointed out that the spectra of GPS and CSS sources, which generally show both high- and low-frequency power laws, cannot be fitted with a model which involves free-free absorption in an evenly distributed absorbing screen since this would imply an exp $(-a\nu^{-2.1})$ cutoff at low frequencies. Clearly, a distribution of optical depths is implied, and we have shown that a simple power-law distribution of the parameter $a = \int n_e^2 T_4^{-1.35}\, dl$ proportional to a^p gives a low-frequency power-law spectrum. We have argued that a distribution of opacities would be produced by thermal instabilities in the radiative bow shock. However, the fact that there is no clear signature of exponential absorption by a uniform shock-photoionized medium, external to the radio source, suggests that this medium is also clumpy and presumably has a two-phase structure. Hence, variable opacity in the preionized ISM and variations in opacity resulting from the shredding of these clouds by the bow shock should also contribute to the overall opacity of the source. As we have emphasized in § 5 the source of the variation in opacity does not affect the general fit to the peak frequency–size relation so that the fit to this relationship is secure. The inference of an absorbing screen with these properties is a feature of the model which can be checked with a three-dimensional radiative shock calculations. We also emphasize that the assumption of a *power-law* distribution of opacities is probably not essential. It is likely that *any* broad distribution of optical depths would suffice.

The depolarization of GPS and CSS sources is an inevitable consequence of this theory. In fact, the estimates of the local rotation measure in § 6 suggest that a large number of field reversals are necessary in order that the integrated rotation measure be as low as observed. Thus, rotation measures inferred from VLBI observations should show a rich and varied structure.

We would like to thank R. S. Sutherland for useful discussions during the course of this work and M. Begelman, the referee of the original manuscript, for numerous constructive comments.

REFERENCES

Akujor, C. E., & Garrington, S. T. 1995, A&AS, 112, 235
Baker, J. C., & Hunstead, R. W. 1996, ApJ, 452, L95
Baker, J. C., Hunstead, R. W., & Brinkmann, W. 1995, MNRAS, 277, 553
Begelman, M. C. 1996, in Cygnus A: Study of a Radio Galaxy, ed. C. L. Carilli, & D. A. Harris (Cambridge: Cambridge Univ. Press), 209
Begelman, M. C., & Cioffi, D. F. 1989, ApJ, 345, L21
Blandford, R. D. 1996, in Cygnus A: Study of a Radio Galaxy, ed. C. L. Carilli & D. E. Harris (Cambridge: Cambridge Univ. Press), 264
Blandford, R. D., & Königl, A. 1989, ApJ, 232, 34
Clarke, D. A. 1996, in ASP Conf. Ser. 100, Energy Transport in Radio Galaxies and Quasars, ed. P. E. Hardee, A. H. Bridle, & J. A. Zensus (San Francisco: ASP), 319
Dallacassa, D., Fanti, C., Fanti, R., Schilizzi, R. T., & Spencer, R. E. 1995, A&A, 295, 27
De Young, D. S. 1993, ApJ, 402, 95
Dopita, M. A., & Sutherland, R. S. 1996, ApJS, 102, 161
Dreher, J. W., Carilli, C. L., & Perley, R. A. 1987, ApJ, 316, 611
Fanti, C., Fanti, R., Dallacassa, D., Schilizzi, R. T., Spencer, R. E., & Stanghellini, C. 1995, A&A, 302, 117
Fanti, C., Fanti, R., Parma, P., Schilizzi, R. T., & van Breugel, W. J. M. 1985, A&A, 143, 292
Fanti, C., et al. 1989, A&A, 217, 44
Fanti, R., Fanti, C., Schilizzi, R. T., Spencer, R. E., Rendong, N., Parma, P., van Breugel, W. J. M., & Venturi, T. 1990, A&A, 231, 333
Gelderman, R. 1994, Ph.D. thesis, Univ. Virginia
Gelderman, R., & Whittle, M. 1994, ApJS, 91, 491
———. 1996, ApJ, in press (GW)
Gull, C. I., Cox, S. F., & Scheuer, P. A. G. 1991, MNRAS, 252, 558
Inoue, M., Tabara, H., Kato, T., & Aizu, K. 1995, PASJ, 47, 725
Kameno, S., et al. 1995, PASJ, 47, 711
Lang, K. 1980, Astrophysical Formulae (Berlin: Springer)
Mantovani, F., Junor, W., Fanti, R., Padrielli, L., & Saikia, D. J. 1994, A&A, 292, 59
Morganti, R., Killeen, N. E. B., & Tadhunter, C. N. 1993, MNRAS, 263, 1023 (TM)
Norman, M. L. 1996, in ASP Conf. Ser. 100, Energy Transport in Radio Galaxies and Quasars, ed. P. E. Hardee, A. H. Bridle, & J. A. Zensus (San Francisco: ASP), 319
O'Dea, C., Baum, S., & Stanghellini, C. 1991, ApJ, 380, 66
O'Dea, C. P., & Baum, S. A. 1996, AJ, submitted
O'Dea, C. P., Baum, S. A., Stanghellini, C., Morris, G. B., Patnaik, A. R., & Gopal-Krishna, 1990, A&AS, 84, 549
Pacholczyk, A. G. 1970, Radio Astrophysics (San Francisco: Freeman)
Phillips, R. B., & Mutel, R. L. 1982, A&A, 106, 21

Readhead, A. C. S., Taylor, A. C. S., Pearson, T. J., & Wilkinson, P. N. 1996, ApJ, 460, 634
Sanghera, H. S., Saikia, D. J., Lüdke, E., Spencer, R. E., Foulsham, P. A., Akujor, C. E., & Tzioumis, A. K. 1995, A&A, 295, 629
Scheuer, P. A. G. 1982, in IAU Symp. 97, Extragalactic Radio Sources, ed. D. S. Heeschen & C. M. Wade (Dordrecht: Reidel), 163
Spencer, R. E., McDowell, J. C., Charlesworth, M., Fanti, C., Parma, P., & Peacock, J. A. 1989, MNRAS, 240, 657
Stanghellini, C., O'Dea, C., Baum, S., Dallacassa, D., Fanti, R., & Fanti, C. 1996a, ApJ, in preparation
Stanghellini, C., O'Dea, C. P., Baum, S. A., & Fanti, C. 1996b, ApJ, in preparation
Stanghellini, C., O'Dea, C. P., Baum, S. A., & Laurikainen, E. 1993, ApJS, 88, 1
Sutherland, R. S., Bicknell, G. V., & Dopita, M. A. 1993, ApJ, 414, 510
Tadhunter, C. N., Morganti, R., Aligheri, diSerego, S., Fosbury, R. A. E., & Danziger, I. J. 1993, MNRAS, 263, 999 (TM)
Taylor, G. B., Inoue, M., & Tabara, H. 1992, A&A, 264, 421
van Breugel, W. 1981, in IAU Symposium 110, VLBI and Compact Radio Sources, ed. R. Fanti, K. Kellerman, & G. Setti (Dordrecht: Reidel), 59
Wall, J. V., & Peacock, J. A. 1985, MNRAS, 216, 173
Wilkinson, P. N., Polatidis, A. G., Readhead, A. C. S., Xu, W., & Pearson, T. J. 1994, ApJ, 432, L87
Williams, A., & Gull, S. F. 1984, Nature, 310, 33